



Case Report

Numerical and Physical Analysis on the Response of a Dam's Radial Gate to Extreme Loading Performance

Iman Faridmehr ¹, Ali Farokhi Nejad ^{2,3}, Mohammad Hajmohammadian Baghban ^{4,*} and Reza Ghorbani ⁵

¹ Institute of Architecture and Construction, South Ural State University, Lenin Prospect 76, 454080 Chelyabinsk, Russia; s.k.k-co@live.com

² Faculty of Engineering, School of Mechanical Engineering, Universiti Teknologi Malaysia (UTM), Johor Bahru 81310, Malaysia; ali.farokhi@polito.it

³ Department of Mechanical and Aerospace Engineering, Polytechnic of Turin, 10129 Torino, Italy

⁴ Department of Manufacturing and Civil Engineering, Norwegian University of Science and Technology (NTNU), 2815 Gjøvik, Norway

⁵ Production Operation Company of Karkheh Dam Hydropower Plant, Andimeshk, Khuzestan 6483169351, Iran; reza_ghorbani1359@yahoo.com

* Correspondence: mohammad.baghban@ntnu.no; Tel.: +47-48-351-726

Received: 27 July 2020; Accepted: 26 August 2020; Published: 29 August 2020



Abstract: Maintaining the reservoir safety of large dams has considerable importance for the public where they are constructed in heavily populated and industrialized areas. The extreme hydrodynamic force caused by ground acceleration, cavitation damage, and vibration are among concerns that threaten the safety of the spillway and its conveyance structures when subjected to a natural disaster, such as earthquakes and severe floods. Current research investigates the hydrostatic and hydrodynamic performance of the Karkheh Dam spillway radial gate through 3-D finite element (FE) models using ABAQUS/Explicit. The common loads applied on the radial gate were reviewed and stress–strain in the skin plate and trunnion were investigated as a result of developed hydrodynamic pressures. The performance of conveyance structures subjected to significant discharge was also investigated through a small-scale model to evaluate the cavitation damage index. The results of this research will help researchers in the field of civil and hydraulic engineering for the risk analysis of the radial gates and conveyance structures.

Keywords: spillway radial gate; hydrodynamic forces; hydrostatic forces; cavitation index; aerator system

1. Introduction

The importance of a safe and reliable dam spillway cannot be ignored; several casualties of dams have been reported by poorly constructed and/or designed spillways or deficient discharge capacity [1–3]. The dynamic reservoir forces developed during a ground acceleration are of importance in the analysis and design of the radial gates. The seismic waves at the base of a dam during a ground acceleration can be significantly amplified at the top of the reservoir. Radial gates may be subject to such enlarged acceleration. This acceleration at the radial gates could be several times bigger than that measured on a rock at the abutment, depending on the location of the spillway gate, the response of the dam structure, actual water head on the gate, flexibility of the gate structure, and whether the transverse, longitudinal, or vertical acceleration is considered.

Besides, spillways for medium-to-high head dams can experience flow velocities as high as 50 m/s. Due to the geometrical deformities and inherent surface roughness of concrete, such spillway conveyance structures are susceptible to cavitation damage. Considering the importance of the spillway

and given the requirement for reliable operation in the extreme loading conditions, the destructive effects of cavitation damage to the conveyance structures, mainly chute, should be prevented.

Standard methods for computing hydrodynamic loads on spillway gates are based on theories developed for concrete dams. In particular, the current practice for computing hydrodynamic loading on dams relies on a method developed by Westergaard for rigid dams [4]. In this approach, the parabolic hydrodynamic pressure distribution over the height of the dam was determined to be the same as a pressure developed by a certain body of water called “added mass”, which is forced to move with the dam during the ground motion. The approximate (simplified) formula of Westergaard for the water pressure is continuously used by the industry in preliminary dam design and the seismic evaluation of spillway gates. Nevertheless, several problems arise with the use of the Westergaard simplified formulation for estimating hydrodynamic interaction force. These problems are summarized as: Pseudo-static methods not accounting for (1) the flexibility of the gates, (2) accurate calculation of the amplification of the ground motion acceleration through the dam, and (3) the three-dimensional effects when the gates are set back from the face of the dam.

Chopra calculated the hydrodynamic pressure on a dam/spillway and its response under horizontal and vertical ground motions of the earthquake; considering the effect of compressibility of the fluid [5]. Gogoi and Maity [6] defined an algorithm for the analysis of a coupled elastic dam–reservoir system composed of an elastic dam and compressible water. The parametric study of the coupled system showed the importance of both the water height of the reservoir and the material properties of the dam. Sasaki et al. [7] studied the basic characteristics of hydrodynamic pressure acting on radial gates during an earthquake based on a numerical analysis that considered the vibration of dam bodies and gates. They proposed a method of calculating hydrodynamic pressure during an earthquake for the seismic performance evaluation analysis of gates. Versluis [8] performed an extensive study on the hydrodynamic loads on large lock gates. In this research, a contribution of sloshing effects on the gates was also investigated and it was determined that such dynamic loads can be neglected. Advanced finite element method (FEA) techniques are now typically applied to determine the hydrodynamic loads on dams and spillway gates, reflecting current reclamation practice [9–15]. In this approach, the reservoir is modeled using solid elements with a fluid equation of state and the dam, foundation, and gates as an elastic structure. The interaction of the reservoir–dam (gate) system is modeled using contact surface elements. The time-dependent analysis allows simulation of dam/gate response to the hydrodynamic load from the reservoir in 3-D space.

Besides, several studies have been conducted to evaluate the performance of conveyance structures subjected to significant discharge. Fadaei Kermani et al. [16] proposed a method to predict cavitation damage on spillways. Serife Yurdagul Kumcu [17] investigated of flow over spillway modeling through the 1/50-scaled physical model. In his study Flow depth, discharge, and pressure data were recorded for different flow conditions. Cavitation risk estimation at orifice spillway based on ultrasonic velocity profiling (UVP) and dynamic pressure measurements have been presented by Michael Pfister et.al [18]. LuoO Yong et.al [19] presented a numerical simulation of aeration and cavitation in high dam spillway tunnels. Cavitation potential of flow on stepped spillways investigated by K. Warren Frizell et.al [20].

In this study, the characteristics of a Karkheh Dam spillway’s radial gate was considered. The Karkheh Dam is a large multi-purpose earthen embankment dam built in Iran in 2001. It is 127 m high with a reservoir capacity of 5.9 billion cubic meters. The Karkheh Dam was designed to irrigate 320,000 hectares of land, produce 520 MW of hydro-electricity, and prevent downstream floods. Figure 1 shows the plan of the dam, reservoir, and spillway.

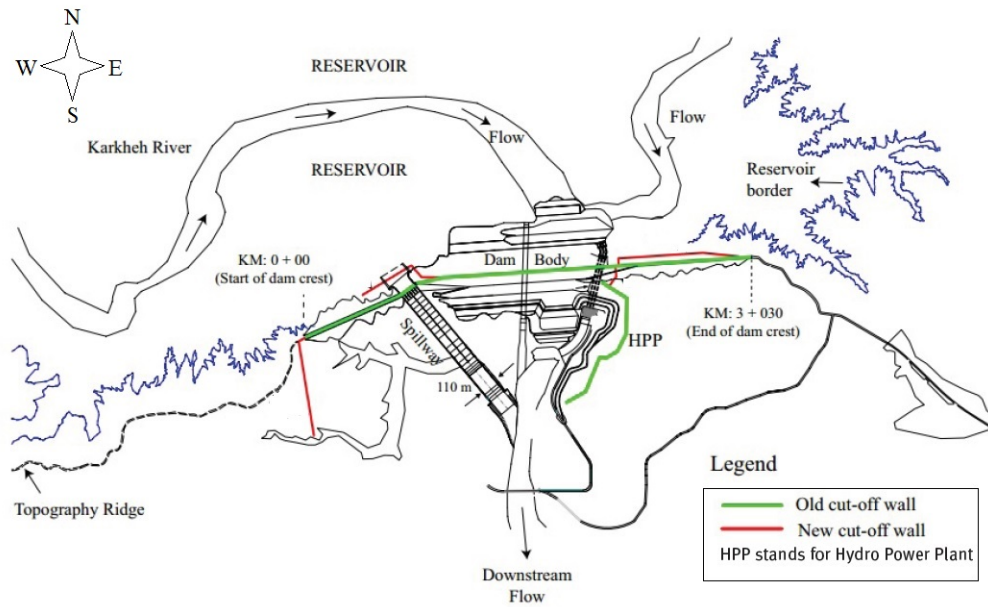


Figure 1. Plan of the Karkheh dam (Andimeshk, Iran), showing old and complementary cutoff wall.

A spillway radial gate is composed of a skin plate connected by trusses to a trunnion or pinned joint that can be rotated about the trunnion to adjust the water flow through hydraulic structures (link rod) as shown in Figure 2a radial (or Taintor) gate acts similarly to a section of a drum. The pressure is transferred from the curved face through the horizontal support beams to the radial arms at the sides of the opening. The arms act as columns and transfer thrust to a common bearing located on either side of the gate opening. Flow is underneath the curved face as the gate is opened. This design results in a lightweight, economical gate that can be opened and closed with minimum effort and with a comparatively small number of turns of the handwheel on the hoist.



Figure 2. Primary radial gate components of Karkheh Dam (a) truss and skin plate, (b) trunnion beam.

Karkheh dam spillway has six radial gates, each 15 m width with a height of 18.29 m (209 m above sea level); constructed generally for flood control with an overall discharge 18,700 m³/s. The structural dimensions of a spillway gate including width, height, skin plate radius, and the location of trunnions have been designed according to specific principles. The location of trunnions has an important function to resist hydrostatic forces. To maintain spillway stability, it is recommended that the hydrostatic resultant force applied to a radial gate possess either horizontal or downward direction to minimize overturn force. Mounting trunnions at one-third radial gate’s height make the direction of resultant force toward the gate horizontal. In general terms, the resultant force tends to be downward for lower trunnion locations. Accordingly, the trunnion locations are recommended to be one-third or half of the

radial gate height. Additionally, the skin plate radius has an oppositional relationship with the weight of the gate. A radial gate with a small skin plate radius requires great force for operation. Generally, the skin plate's radius should be equal to or 20% higher than the height of the gate. Figure 3 shows the geometrical features of the Karkheh Dam's radial gate.

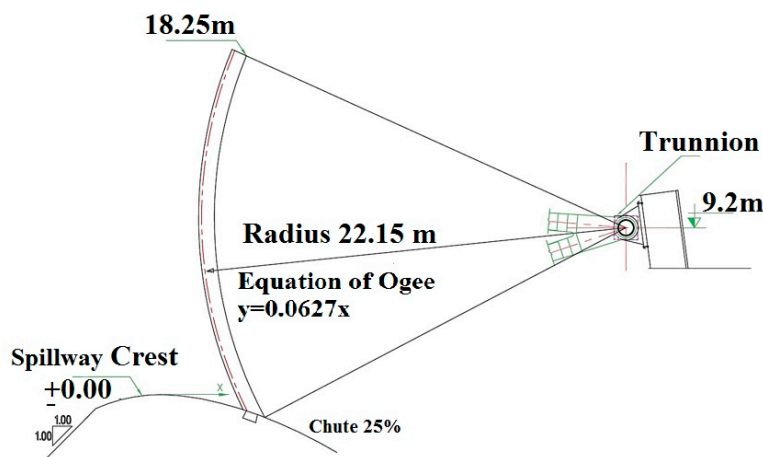


Figure 3. Geometric characteristics of Karkheh Dam's radial gate spillway (m).

In this research, the structural performance of Karkheh Dam spillway's radial gate subjected to hydrostatic and hydrodynamic loading was evaluated through 3-D finite element (FE) models using ABAQUS/Explicit. Additionally, the performance of conveyance structures, chute, and aerator systems, subjected to normal and severe discharge were evaluated through a small-scale physical model of the spillway.

2. Materials and Methods

2.1. Applied Load on Radial Gate Spillway

Radial gates in the closed position can be exposed to a variety of loads, including hydrostatic pressure, ice loads, and hydrodynamic forces, as results of dam–reservoir seismic waves [21]. Additionally, several other loads are developed during the gate operation, including vibration and bending moment, as a result of trunnion pin erosion. The determination of hydrodynamic loads on spillway gates is a complex process that involves the seismic response of the dam, response of the spillway gates, and the response of the reservoir water. Unfortunately, it is difficult to determine their value and location precisely due to their specific nature. Therefore, designers should make an engineering judgment to predict accurately based on recognized resources and engineering experiences. Generally, the following forces apply to radial spillway gates:

- i. Gravity forces (the structural dead load) and hydrostatic force;
- ii. The hydrodynamic forces applied to radial gates as a result of the earthquake, wind, severe flood, etc.

The dead load is calculated based on the weight of the materials used in the construction of the gate and its related components. Dead loads are the weight of the gate's permanent components which act on the center of gravity. In the case that gates have been smeared in sludge or sediment during operation, the weight of this sediment is added to the weight of the gate. Generally, gates have been made of materials like steel with an approximate specific weight of 77 kN/m^3 . According to the calculations, 67 kN is applied to the center of gravity of the Karkheh Dam's radial gate due to the weight of the materials.

The forces applied on the radial gate from water can be divided into two categories: hydrostatic and hydrodynamic. Hydrostatic forces are static forces as a result of upstream water applied to the

radial gate. The magnitude of hydrostatic loads applied on the radial gate can be varied due to the rise or fall of the upstream during a flood or low rainfall months. Hydrodynamic forces are generally formed as a result of the strong waves hits to radial gates during extreme loading conditions (i.e., earthquake where the reservoir is full). Estimation of the period of earthquakes reoccurrence in a particular area requires knowledge of the seismic features of the area. According to the International Committee On Large Dams ICOLD 1998 [22], there are three seismic levels with different peak ground acceleration (PGA) (Table 1).

Table 1. Peak ground acceleration (PGA) for different seismic levels.

Seismic Design Level	Return Period (in Years)	Maximum Peak Ground Acceleration (g)	
		Horizontal (PGA H)	Vertical (PGA V)
Design Base Level (DBL)	500	0.29	0.18
Maximum Design Level (MDL)	1000	0.39	0.27
Maximum Credible Level (MCL)	Deterministic	0.54	0.44

In this study, the earthquake analysis was based on the maximum credible earthquake level (MCL) scenario. In this loading condition, the structure can have serious/un-repairable structural damages without the sudden release of the reservoir's water. The earthquake event (acceleration history) was taken from the seismic hazard study and applied in the non-linear dynamic analysis. Based on the previous reports provided, the most critical earthquake of the existing dam in MCL is the Manjil record. Figure 4 shows the horizontal component of the Manjil ground motion scaled for MCL.

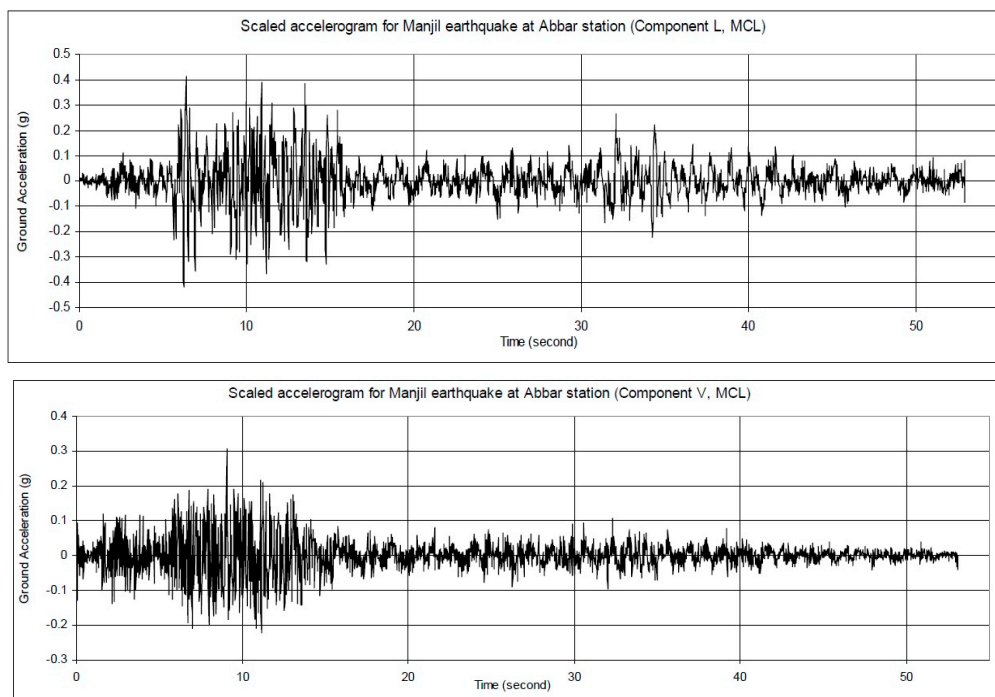


Figure 4. Scaled Manjil ground motion recorded at Abbar station (horizontal component L and vertical component V).

2.2. Finite Element Simulation

2.2.1. 3D Model Generation

In the first stage, the 3D model of the radial gate was created in Abaqus/Explicit. This particular model involved over 485 components, which reveals the geometrical complexity of the structure.

The thickness of the skin plate, considering the corrosion, was taken to be 2 mm less than the initial size. Figures 5 and 6 illustrate the details of the trunnion dimension and skin plate, respectively. To generate the solid part of the 3D model, the shell element with 4 nodes and reduce integration point (S4R) ability was used, in which the solid parts include 60,753 S4R elements. The mesh quality was evaluated based on geometrical criteria (e.g., element aspect ratio, element skew angle, minimum, and maximum angle of the element) [23].

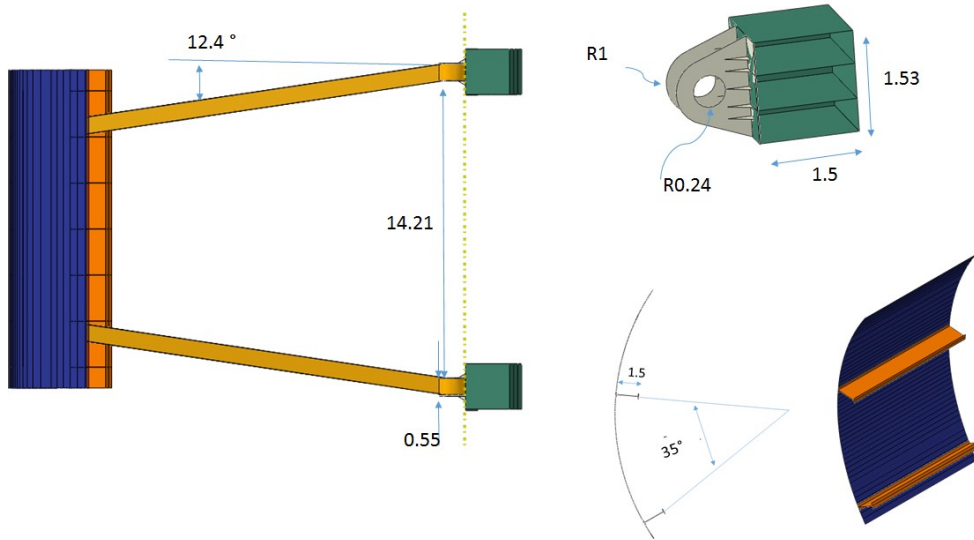


Figure 5. Dimensions of trunnion and arms.

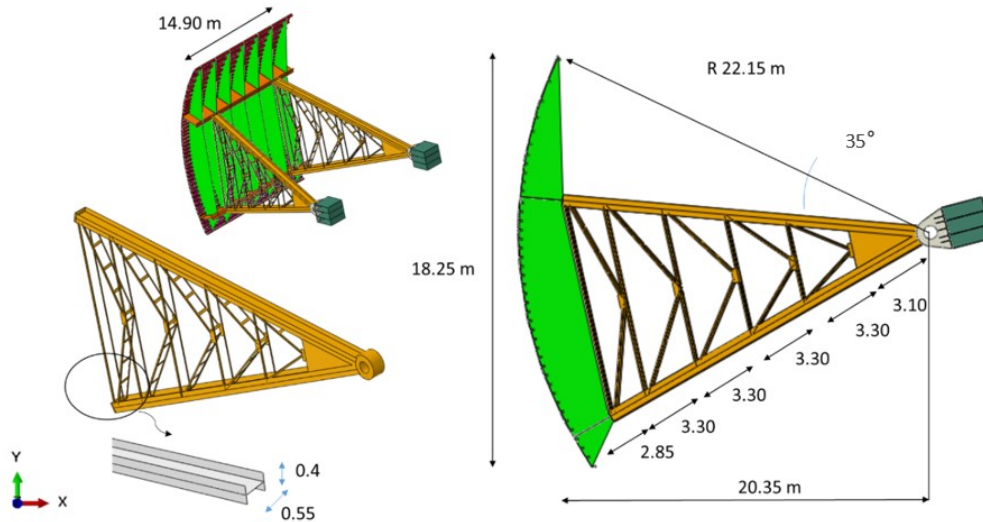


Figure 6. Dimensions of skin plate and arms.

2.2.2. Material Properties

According to the available documents, it is evident that the ST-52 steel sheet has been employed in many existing radial gates. The non-linear behavior material properties were modeled in the software by the use of the true stress–strain curve [24]. Based on the introduced stress–strain curve, the nonlinear behavior of the material was imported into ABAQUS as tabulated data. The table contains yield stress and plastic strain of every load incrementation from the tensile test machine. Table 2 shows the general features of ST-52 material properties.

Table 2. Material properties of ST-52.

Density (kg/m ³)	Elastic Modulus (GPa)	Initial yield Stress (MPa)	Ultimate yield Stress (MPa)	Strain Hardening Coefficient	Failure Strain (%)
7850	210	330	460	0.25	33

2.2.3. Modal Analysis

Because of the complications caused by numerous components of the model as well as the concern of precise welding between various components, frequency analysis could be used to reveal the strength of the structure. In other words, the accuracy of connected components could be verified through frequency analysis and mode shapes [25]. To this end, the modal analysis performed in this study was a verification test for controlling the connections between all connected parts. It is well recognized that when a complex system has many components, the best way to control the connectivity between different parts can be done by extracting the natural frequency of the system. If the natural frequency is very low and the first mode shape is not a normal predicted mode shape (pure bending or torsion mode), it represents that discontinuity exists in the model and the model should be amended. After some trial attempts, the perfect model can be reached. In this study, the center of rotation was constrained to the trunnion supports and it was fixed in all degrees of freedom as the only boundary condition of this simulation. The first and second modes of a structure can provide considerable insight into the strength of the structure against bending or twisting. Figure 7 shows the first and second mode shapes of modal analysis, which reveal the fact that an appropriate connection was set up among different components. Additionally, the first mode indicates that the radial gate possesses low bending capacity when subjected to its resonance frequency. This phenomenon is common in radial gates with a truss structure. Based on the frequency and modal analysis of the structure, it was evident that the first and second modes of frequency are related to the structure's strength. The minimum displacement can be observed at the trunnion support due to the effect of fixed boundary conditions. However, in reality, the weight and stiffness of this part are much higher than the other parts of the structure.

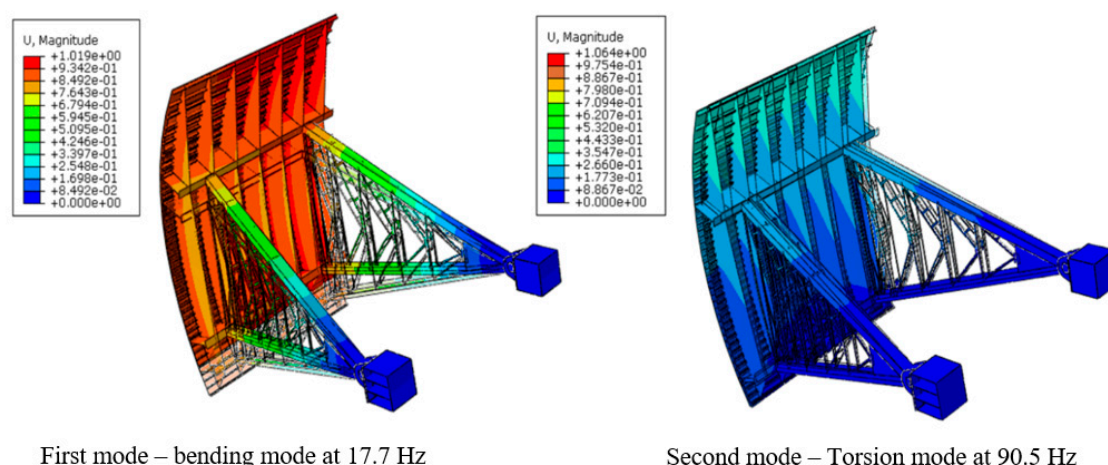


Figure 7. First and second mode shapes of modal analysis.

2.2.4. Coupled Acoustic–Structural Analysis

To model the hydrostatic or hydrodynamic pressure applied to the gateway, a coupled acoustic–structure analysis was carried out. In this model, acoustic media was used with water properties. To apply hydrostatic and hydrodynamic (Westergaard criteria) pressure, a constant load was applied to the inner part of acoustic media and it will be transferred to the steel shell of the slipway gateway. To model the hydrodynamic (as a shock wave) pressure, an incident wave regarding

maximum amplitude and decay time was performed. The maximum amplitude and decay time were used from the Manjil earthquake recorded data. Generally, to convert seismic records to the applied loading, a fast Fourier transform (FFT) method is used and the ground acceleration is converted from the acceleration–frequency curve to the spectral acceleration–time period curve [26,27]. Figure 8 illustrates the power spectrum acceleration curve for horizontal and vertical ground motion.

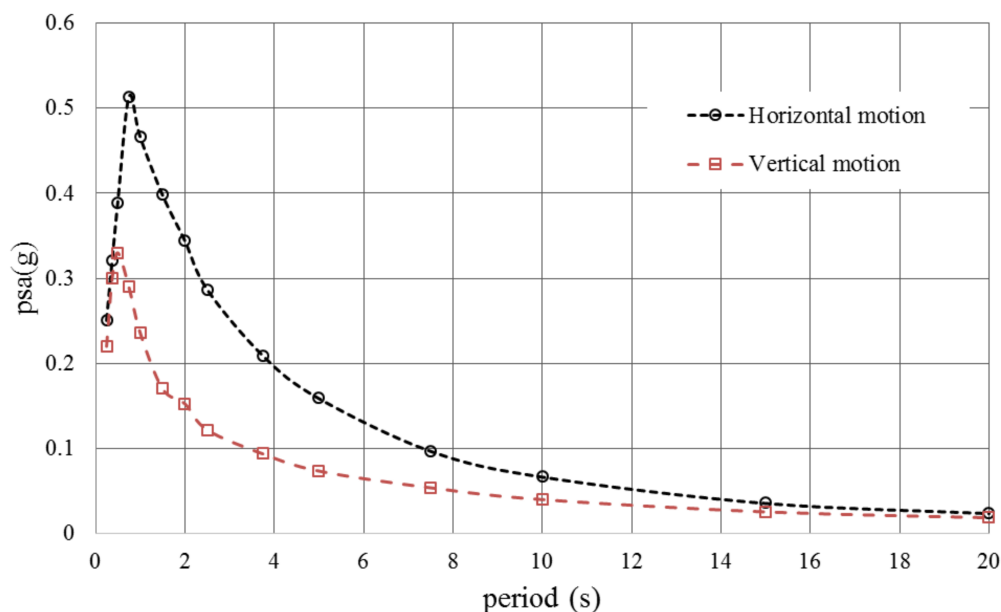


Figure 8. Power spectrum acceleration (psa)–time graph for horizontal and vertical ground motion.

In this study, the horizontal acceleration was taken into account as the maximum applied force. Acoustic volumetric acceleration loads corresponding to the incident wave were then applied to the fluid surface, while the incident wave pressures were applied to the structural surface. The resulting hydrostatic pressure acts perpendicular to the corresponding surface. Thus, positive and negative buoyancy, resulting from the curvature of the radial gate, was taken into account. The influence of the water in the reservoir was considered by modeling the reservoir with fluid elements (second-order brick elements of type AC3D20) according to Figure 9. The reservoir is connected to the upstream surface of the dam utilizing so-called tie constraints. The compressibility of the water in the reservoir was taken into account also. The bulk modulus and density of water for this study were 2.315×10^9 N/m² and 997 kg/m³, respectively. At the rear boundary of the water body—the reservoir—a “viscous” or non-reflecting boundary was used to prevent reflection from this surface. At the bottom boundary of the water body (i.e., the transition from water to rock), 50% absorption due to sediments in the reservoir was assumed. To model the slipway skin, the shell element with reduced integration (S4R) was used. The interface between the metallic part and fluid was coupled with the tie constraint property. The trunnion’s axis of rotation was tied with hinge holes and the central point of the axis was constrained in all degrees of freedom. Figure 9 represents the FE model in detail.

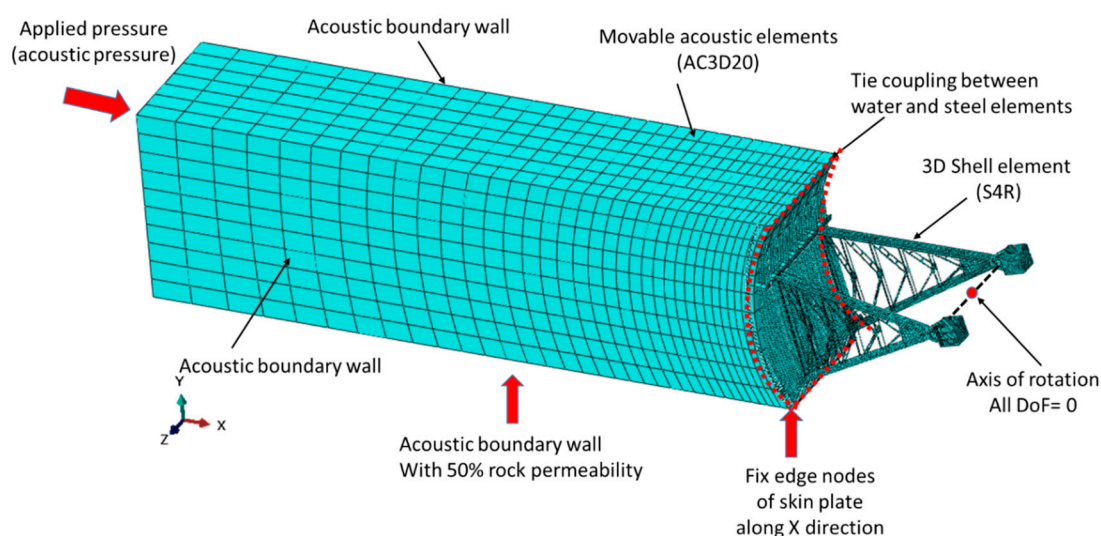


Figure 9. The coupled acoustic–structure finite element model of the slipway gateway.

3. Results and Discussion

3.1. Structural Performance

3.1.1. Results of Hydrodynamic and Hydrostatic Forces

According to the calculations, the results of the hydrostatic and hydrodynamic forces acting on the spillway gate are shown in Table 3. As shown in Table 3, the hydrodynamic force, as a result of the MCL earthquake, imposes a 72% extra load on the spillway compared to hydrostatic force.

Table 3. Applied hydrostatic and hydrodynamic forces to the spillway.

Horizontal Hydrostatic Pressure (FHS)	Vertical Hydrostatic Pressure (FVS)	Resultant of Hydrostatic Forces (FRS)	Angle with Horizon (θ)	Equivalent Hydrostatic Pressure (PHS)	Design Basic Level (DBL) PGA = 0.29 g		Maximum Credible Level (MCL) PGA = 0.54 g	
					FHD Hydro Dynamic Force	Ratio of $(F_{HD} - F_{RS})/F_{RS}$	FHD Hydro Dynamic Force	Ratio of $(F_{HD} - F_{RS})/F_{RS}$
(KN)	(KN)	(KN)	(deg)	(kPa)	(KN)	%	(KN)	%
13,390	3130	13,760	13.2	96.89	20,390	48%	23,750	72%

Peak ground acceleration (PGA).

3.1.2. Nonlinear Performance Using Incident Wave

To apply real models of earthquakes that hit the structure, an impact wave was employed where applied force extracted from a shock spectrum of Manjil ground motion hit the structure in a tiny period of time. The solver of this simulation was dynamic/implicit to capture the stress–strain rate over time. The main difference of this analysis with non-linear hydrodynamic analysis is to provide results over time, rather than ultimate stress and strain, in which residual stress can be identified. Figure 10 shows the shock response of the radial gate subjected to an earthquake wave of Manjil ground motion (MCL level). The stress in the trunnion and horizontal stiffeners, which have the maximum stress in the structure, are around 347 and 334 MPa, respectively. Additionally, it is evident that the relatively high stress was distributed across all of the radial gate’s skin plate. Therefore, it was necessary to evaluate the strain distribution in the radial gate. Figure 11 shows the value of plastic strain in trunnion as 0.014 and the maximum deflection that takes place in the skin plate crest is around 3.7 mm, which is classified as permanent deformation.

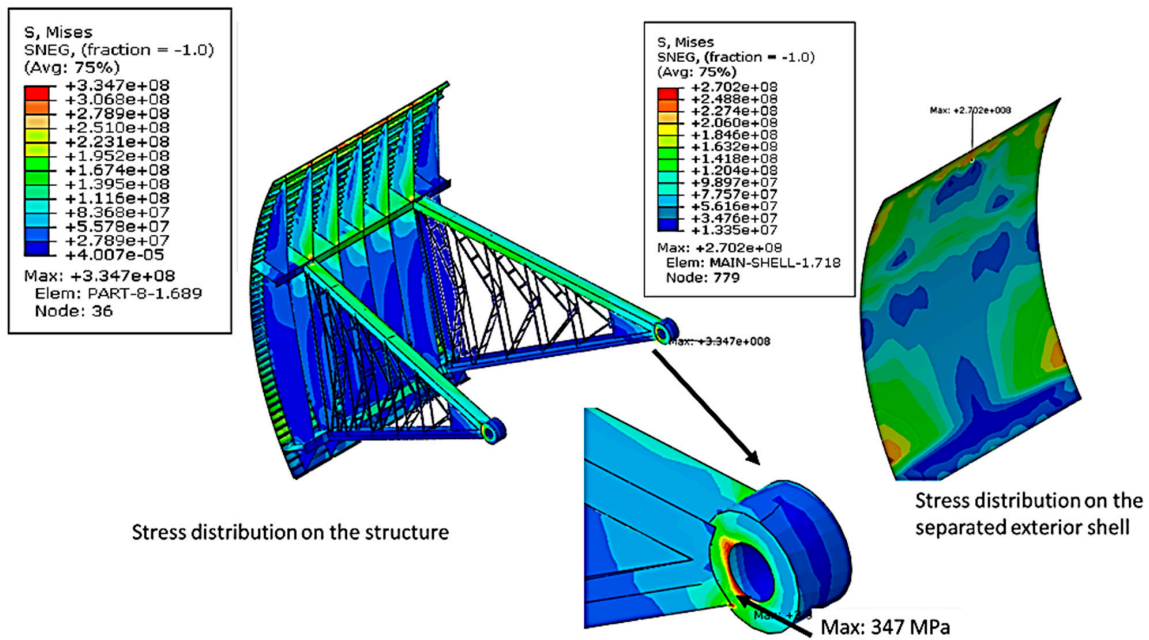


Figure 10. Stress distribution as a result of the shock wave (MCL earthquake).

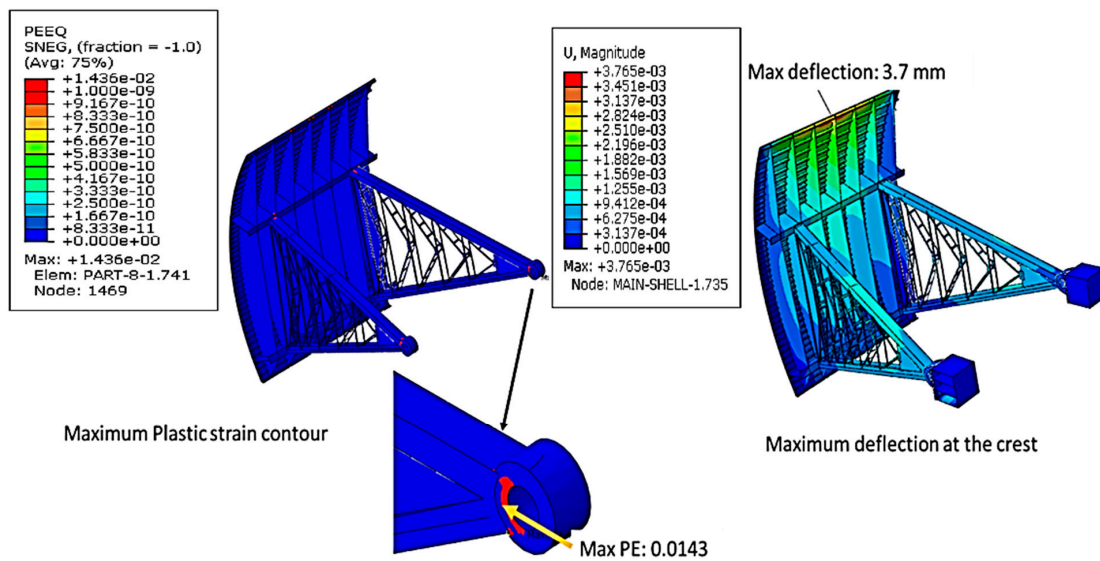


Figure 11. Strain and displacement distribution as a result of a shock wave (MCL earthquake).

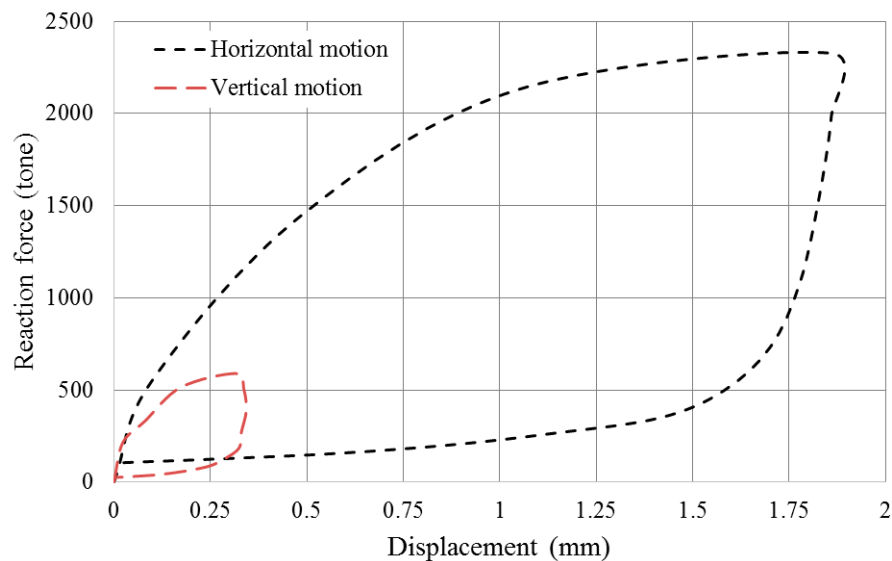
3.1.3. Residual Stress and Hysteresis Curve

The results of maximum stress and strain in various loading protocols are illustrated in Table 4. A comparison between the corresponding strain from hydrodynamic analysis and the other simulations illustrates that the radial gate experiences significant plastic strain as a result of hydrodynamic forces. According to ICOLD regulation, a combination of hydrostatic and MCL earthquake consider as an extreme loading condition. ICOLD recommended taking into account the factors of safety of 1 for the dam body. Applying such a safety factor for the radial gate spillway, it can be concluded that the radial gate is vulnerable to incident wave where the stress at the trunnion surpasses the yield stress (330 MPa).

Table 4. Stresses, strain, and deflection magnitude at different loading protocols.

Case	Stress at Trunnion (MPa)	Stress at Skin (MPa)	Stress at Stiffener (MPa)	Plastic Strain %	Maximum Deflection (mm)
Hydrostatic	269	101.2	208.4	0	1.9
Hydrodynamic (144 years period)	310	139	287.2	0	2.6
Hydrodynamic (500 years period)	331	220	304	0.04	3.6
Incident wave	335	320.8	330	2.7	3.75

Analysis results of the impact wave reveal the fact that the structure experienced significant residual stress. Figure 12 investigates the hysteresis curve of the radial gate subjected to the MCL earthquake. The area inside of the black curve shows the horizontal hysteresis energy absorbed by the structure during the loading and unloading process. The most portion of transfer energy to the structure is in the horizontal direction; however, the vertical side also is not negligible (red curve). The maximum deformation corresponding to the horizontal reaction force is around 1.8 mm, which becomes null after unloading. It shows that the overall response of the structure is elastic and localized deformation occurred.

**Figure 12.** Hysteresis curve as a result of an impact wave due to an MCL earthquake.

To monitor stress fluctuations over time, the time history of stress was taken into account, as shown in Figure 13. This figure illustrates that an average of 100 MPa stress remains in the structure in the aftermath of the impact wave, and will significantly decrease the radial gate capacity to resist against secondary waves. Furthermore, the superposition of this residual stress to stress from hydrostatic analysis clearly shows the vulnerability of the radial gate to an impact wave due to an MCL earthquake.

Moreover, the green area of Figure 13 represents the plastic residual stress that will remain in the structure as the permanent deformation. The stress level in Figure 13 after 10 s shows that the stress level will have remained around 100 MPa, and this value is equivalent to the accumulated energy inside of the black curve from Figure 12. This confirms that the whole structure is in the elastic condition; however, the maintenance procedure to control the welded region and non-destructive test (NDT) inspection should be performed immediately after impact loading.

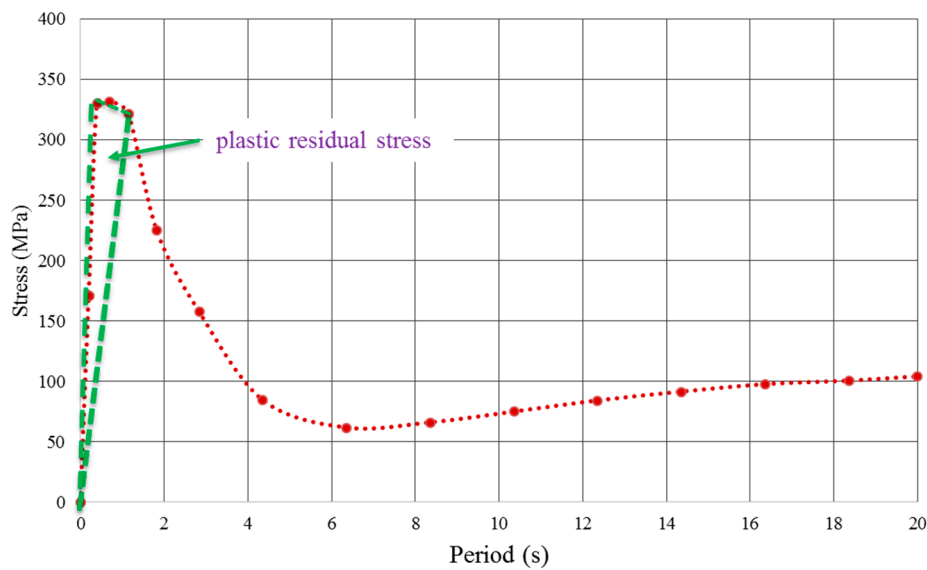


Figure 13. Stress history over time as a result of an impact wave due to an MCL earthquake.

3.2. Hydraulic Performance

The conveyance structures (chute) connected to the spillway crest is subject to huge flows with high velocities in the case of radial gate failure due to earthquake impact waves. In this section, the performance of a chute and aeration system was evaluated in the case of normal and extreme discharge through a small-scale model of the Karkheh Dam spillway.

Cavitation is the main hydraulic damage in the case of the extreme release of a dam reservoir with high velocity. Generally, the cavitation phenomenon will take place when the local pressure in flowing water drops below the vapor pressure, and bubbles or cavities form locally in the body of flow. In the case that cavitation bubbles undergo high local pressure, they collapse. Collapsing the cavitation bubbles in the vicinity of solid boundary release an extremely high pressure on a small surface over a short period of time [27]. Consequently, a solid surface receives a hole, so-called cavitation pitting. Several cases of cavitation damage in a chute of spillways documented [17,28,29]. The flow pressure and velocity are the main parameters to evaluate the cavitation potential as shown in the following equation [28,30]:

$$\sigma = \frac{p - p_v}{\frac{\gamma_w V^2}{2}} \tag{1}$$

where σ is cavitation index and it is a dimensionless parameter. p is the pressure at the flow surface (atmospheric pressure plus hydrostatic pressure ($\frac{N}{mm^2}$)); P_V is the vapor pressure of water, which is temperature function; γ_w is the density of water ($\frac{1000 \text{ kg}}{m^3}$); V is the average flow velocity (m/s).

Table 5 shows different levels of cavitation damage risk and the equivalent cavitation index based on the flow velocity.

Table 5. Cavitation damage index [31].

Level	Cavitation Damage Risk	Flow Velocity (m/s)	Cavitation Index
1	No cavitation damage	$V \leq 5$	$\sigma > 1$
2	Possible cavitation damage	$5 < V \leq 16$	$0.45 < \sigma \leq 1$
3	Cavitation damage	$16 < V \leq 25$	$0.25 < \sigma \leq 0.45$
4	Serious damage	$25 < V \leq 40$	$0.17 < \sigma \leq 0.25$
5	Major damage	$40 > V$	$0.17 > \sigma$

In the Karkheh Dam's spillway, by taking into account the levels of upstream and downstream, three aeration systems were mounted on the spillway's chute to prevent possible cavitation damage. An aeration system consists of two main components: an air supply system and a surface discontinuity that entrains the air into the flow. The head loss in the flow determines the dimension of the inlet duct. Several parameters should be considered for designing the aeration system, including the air concentration on the floor downstream of the aerator, the air demand from the aerator, the water jet length, and the difference between the atmosphere and air pressure beneath the nappe [32,33]. An aerator normally works by causing the flow to separate from the invert of a channel to form a large air cavity (distinct from the small cavitation bubbles which are usually filled with water vapor). As the water passes over the cavity, the air is entrained through the lower surface of the flow by the effects of turbulence and drag. It has also been found that strong entrainment can occur through the free surface due to the sudden pressure changes and turbulence that the aerator induces within the flow. Existing guidelines on aerator spacing and slope change are mostly based on model and prototype observations of the rate at which air concentration decreases with distance. According to the literature, typical distances between aerators were suggested to be in the range of 30 to 100 m. Nevertheless, the dimensionless cavity length, cavity pressures, and air entrainment coefficient, as shown below, are significant parameters for adjusting the slope and spacing the aeration system along with the spillway chute.

- Cavity length

$$\lambda = \frac{L}{d_0} \quad (2)$$

where L is cavity length; d_0 is water depth; and λ is dimensionless cavity length.

- Air entrainment coefficient

$$\beta = \frac{Q_a}{Q_w} \quad (3)$$

where Q_a is air flow rate (m^3/s); Q_w is discharge through spillway (m^3/s); and β is air entrainment coefficient.

- Cavity pressure

$$P_n = \frac{\Delta p}{\rho g d_0} \quad (4)$$

where Δp is average cavity pressure (N/m^2); ρ is the density of water; g is the gravitational acceleration; and P_n is dimensionless cavity pressures.

In the Karkheh Dam's spillway, the total length of the chute from the stilling basin to spillway crest is 662.59 m. The initial longitudinal slope of the chute, at the 173.58 m beginning length from the crest, is 25% that with a 110 m radius arc connected to the first aerator. After that, by using a 5% slope and a 373 m distance, the chute is connected to the second aeration system. After the second aeration system, the chute, having a parabolic curve ($y = 0.05x + 0.002x^2$), is connected to the third aeration system and, finally, to the stilling basin. Figure 14 illustrates the details of the Karkheh Dam spillway's chute and aeration systems.

To evaluate the hydraulic parameters, such as flow velocity in aerators, discharge capacity, and air pressure in aerator ducts stream along with flow pattern, a 1/64 scale model of the Karkheh Dam's spillway was constructed (Figure 15) and the test results verified against analytical calculation. Different equipment, such as piezometer (measure flow pressure), pitot tube (measure flow velocity), and barometer (measure air pressure), were employed to record hydraulic parameters.

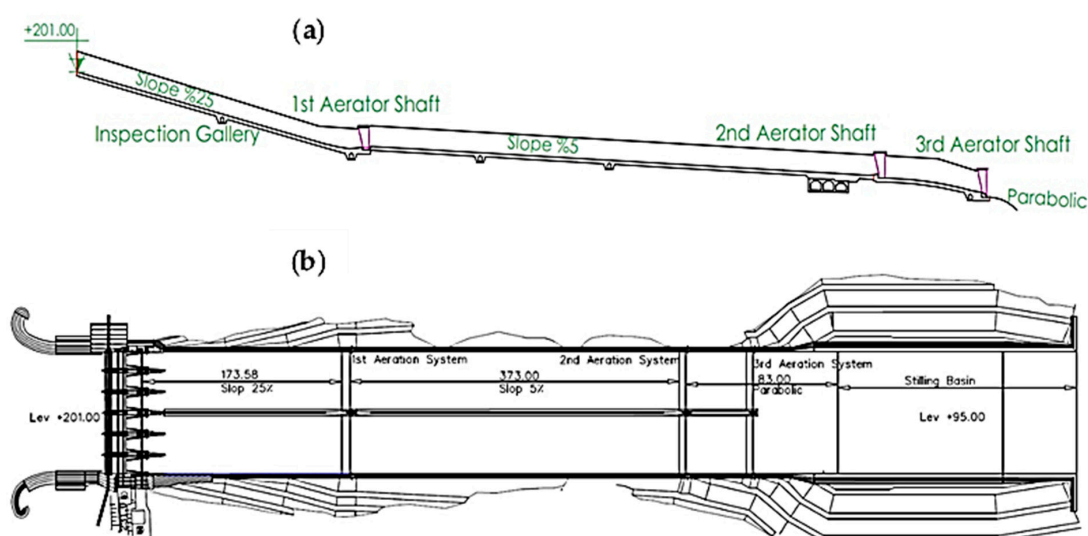


Figure 14. Chute and aeration system of the Karkheh Dam: (a) Section view, (b) plan view.



Figure 15. The 1/64 scale model of the Karkheh Dam's spillway.

The experimental test was set up according to the theory of similarity between prototype and small-scale model, in which the calculation of model parameters and processing of results were prepared accordingly. Granados et al. [34] investigated two- and three-dimensional numerical models along with a small-scale test to simulate water flow behavior over the new Niedów barrage in South Poland. Since the Niedów reservoir is too large, they reproduced only 500 m of the reservoir at a length scale ratio of 27. In their study, the relationship between prototype and small-scale followed the Froude similarity and Reynolds number Re_m criterion [35]. In general terms, Reynolds's number deals with the relationship between frictional and inertial forces, while the Froude number deals with the relationship between gravity and inertial forces. The Re_m number of the laboratory model is determined using the following equation:

$$Re_m = \frac{V_m h_m}{\nu_m} \quad (5)$$

where V_m is the average water velocity; h_m is the water depth of the model before the ogee weir; and ν_m is the kinematic water viscosity. To ensure a hydraulic similarity between the model and the prototype, the Re_m number in the cross-section of the reservoir, before the spillway, was measured and checked against the prototype.

In the current study, the small-scale model of the spillway was constructed using Plexiglas with a roughness coefficient of 0.008 compared to a roughness coefficient of concrete 0.014 [36]. Additionally,

the experimental test was operated according to Froude law similarity regardless of surface tension and viscous force. Scale effects are expected for an air–water flow model in laboratory conditions, since Weber and Reynolds similarity cannot be achieved together with Froude similarity. Several researchers indicate that if the Reynolds number is greater than 10^5 , air entrainment is not affected by the scale of the Froude model [37]. Reynolds numbers between 8.16×10^4 and 1.73×10^5 for the main flow in the chute were considered in the hydraulic model tests. Therefore, scale effects will be expected in the experimental observations. Accordingly, to eliminate the scale effects on air entrainment rate in the small-scale model, the following equation proposed by Kokpinar and Gogus [38] was used according to data extracted from the prototype:

$$\beta = 4.407(\beta_m)^{1.264} \quad (6)$$

where β and β_m are the prototype and model values of the air entrainment rates, respectively. Table 6 summarizes the hydraulic parameters in all three aeration systems of Karkheh Dam's spillway for two different discharge.

Table 6. Hydraulic parameters resulted from the 1/64 scale model.

Cavitation Index on the Floor Downstream of the Aerator	Air Concentration on the Floor Downstream of the Aerator	Air Velocity in Aerator Duct	Air Entrainment	Difference between the Atmosphere and Air Pressure in Aerator Duct	Water Jet Length	Flow Depth in Aerator Duct	Flow Velocity in Aerator Duct	Spillway Discharge
	(%)	(m/sec)	(m ³ /sec)	(m.W.C)	(m)	(m)	(m/sec)	(m ³ /sec)
First Aeration System								
0.30	46.50	43.40	1736	0.197	23.10	0.70	26.95	2000
0.317	18.10	66.10	2644	0.457	30.80	3.50	32.3	12,000
Second Aeration System								
0.51	34.20	36.10	1042	0.071	18.70	0.92	20.51	2000
0.23	23.70	93.20	3730	0.909	46.60	3.40	33.30	12,000
Third Aeration System								
0.43	33.50	25.20	1006	0.062	15.30	0.86	21.94	2000
0.18	38.40	119.10	4765	1.39	49.90	3.25	34.83	12,000

Table 6 summarizes:

- i. The water jet length in the third aerator compared to the prior aerators experience a substantial increase as a result of the convex arc at the bottom of the chute.
- ii. The difference between the atmospheric pressure and aeration channel in the 12,000 $\frac{m^3}{s}$ discharge is clear in all three aeration systems.
- iii. Generally, the velocity and volume of air entrainment in the aerator ducts for 12,000 $\frac{m^3}{s}$ spillway discharge is much higher compared to 2000 $\frac{m^3}{s}$ discharge; particularly in the last aerator.
- iv. The air concentration on the floor downstream of the aeration system for the 2000 $\frac{m^3}{s}$ spillway discharge is relatively high compared to 12,000 $\frac{m^3}{s}$ discharge, especially in the first aerator.
- v. For 12,000 $\frac{m^3}{s}$ spillway discharge, the cavitation index is critical, particularly in the last aerator.

Several researchers propose different methods to evaluate aeration efficiency in spillways. It is known from the published literature that the air entrainment rate for conventional aerators is mainly a function of the upstream Froude number. Ahmed A. Sattar et al. [39] presents the novel application of artificial intelligence methods to evaluate the aeration efficiency over stepped weir for the three flow regimes. They suggest a coefficient to determine the effective variables affecting aeration efficiency. The air entrainment rate, related to the following non-dimensional parameters, as a result of the dimensional analysis for a bottom-inlet aerator [40] is:

$$\beta = 0.29(F_r - 1)^{0.62} \left(\frac{D^2}{h} \right)^{0.59} \quad (7)$$

where β is the air entrainment rate—defined as a ratio of the air discharge supplied by the aerator to the water discharge in the flume; F_r is the upstream Froude number defined as the ratio of the inertia forces to the gravity forces and calculated by the following equation:

$$F_r = U_w / (gh)^{1/2} \quad (8)$$

where U_w is the approaching flow velocity (in m/s), g is the gravitational acceleration (in m/s²), h is the approaching flow depth, and D is the diameter of the aeration holes. Figure 16 shows the variations of the air entrainment rate β with Froude number F_r for all three aeration systems of Karkheh Dam, presented in Table 5 for two spillway discharge. Figure 16 indicates that F_r has an increasing effect on the air entrainment of the aerator.

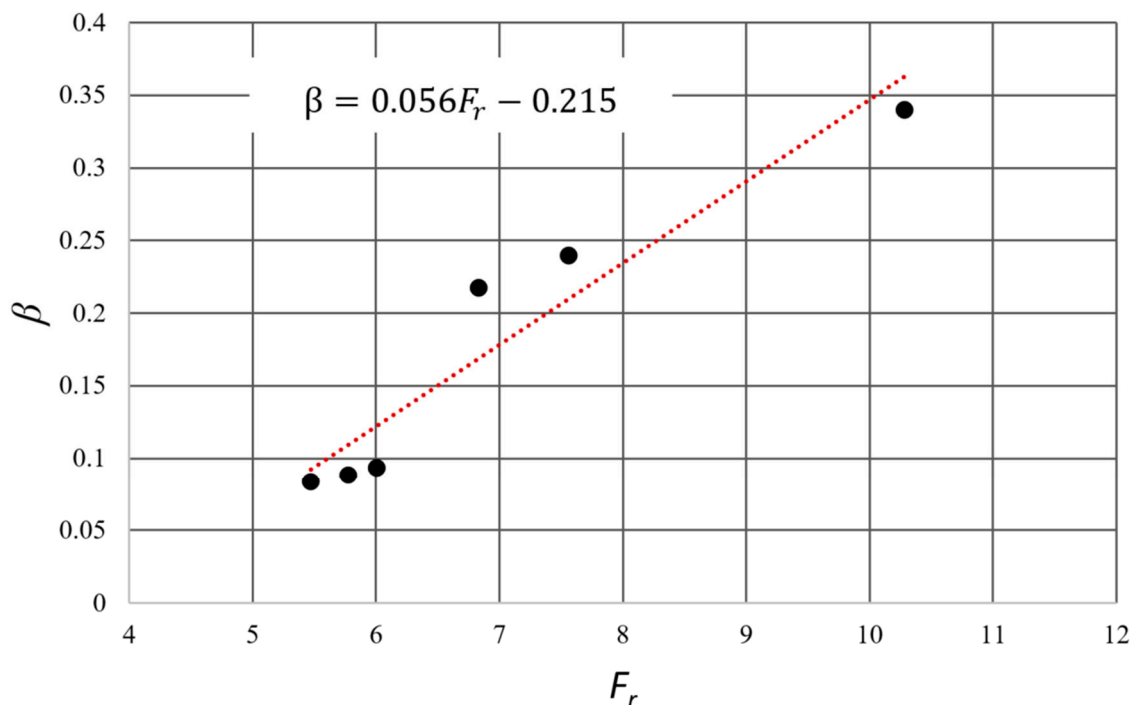


Figure 16. Variations of the air entrainment rate with Froude number.

4. Concluding Remarks

In this study, the structural and hydraulic performance of Karkheh Dam's spillway was investigated in the case of normal and extreme conditions. The primary conclusions are as follows:

- i. The hydrostatic analysis showed an almost acceptable performance for the radial gate however, the hydrodynamic force, as a result of the MCL earthquake, imposes a 72% extra load on spillway compared to hydrostatic force.
- ii. To simulate the real condition for the slipway gateway subjected to the hydrodynamic loading, a coupled acoustic–structural analysis was carried out to model the effect of incident waves on the steel structure.
- iii. Nonlinear performance evaluation using an impact wave theory, equivalent to an MCL earthquake, revealed a high-stress ratio distribution across almost all of the radial gate components. Additionally, plastic strain in the trunnion (0.014) was classified as a permanent strain. Meanwhile,

an average of 100 MPa stress remains in the structure in the aftermath of the impact wave and will significantly decrease the radial gate capacity to resist against secondary waves.

- iv. Aeration efficiency mainly depended on the air entrainment rate. The air entrainment rate itself is a function of the upstream Froude number. The results of this research indicate that increasing the Froude number will increase the air entrainment rate on aerator systems.

Author Contributions: Original draft preparation, numerical models, validation, and methodology: I.F.; supervision, review, and editing: M.H.B.; numerical simulation and time-history analysis: A.F.N.; experimental test: R.G. All authors have read and agreed to the published version of the manuscript.

Funding: This work was supported by funding from The Norwegian University of Science and Technology (NTNU).

Conflicts of Interest: The authors declare no conflict of interest.

References

1. Dubler, J.R.; Grigg, N.S. Dam Safety Policy for Spillway Design Floods. *J. Prof. Issues Eng. Educ. Pr.* **1996**, *122*, 163–169. [[CrossRef](#)]
2. Barfuss, S.L.; Crookston, B.M. Public Safety and Unauthorized Extreme Activities at Spillways. 2018. Available online: <https://digitalcommons.usu.edu/cgi/viewcontent.cgi?article=1183&context=ishs> (accessed on 29 August 2020).
3. Lempérière, F. Dams and floods. *Engineering* **2017**, *3*, 144–149. [[CrossRef](#)]
4. Westergaard, H.M. Water pressures on dams during earthquakes. *Trans. ASCE* **1933**, *95*, 418–433.
5. Fenves, G.; Chopra, A.K. Earthquake analysis of concrete gravity dams including reservoir bottom absorption and dam-water-foundation rock interaction. *Earthq. Eng. Struct. Dyn.* **1984**, *12*, 663–680. [[CrossRef](#)]
6. Gogoi, I.; Maity, D. Seismic safety of aged concrete gravity dams considering fluid-structure interaction. *J. Earthq. Eng.* **2005**, *9*, 637–656. [[CrossRef](#)]
7. Sasaki, T.; Iwashita, T.; Yamaguchi, Y. Calculation Method of Hydrodynamic Pressure in Seismic Response Analysis of Gates. In Proceedings of the Tirthy-Ninth Joint Meeting of UNJR, Kii-Katsuura, Japan, 7–9 November 2007.
8. Versluis, M. Hydrodynamic pressures on large lock structures. *Delft. Delft Univ. Technol* **2010**. Available online: <https://repository.tudelft.nl/islandora/object/uuid:efbc60e5-4c0c-4dd6-a73c-89bfb67b1f6b> (accessed on 29 August 2020).
9. RamaRao, V.S.; Bhajantri, M.R. Performance of modified spillway for heightened gravity dam. *ISH J. Hydraul. Eng.* **2020**, *26*, 325–331. [[CrossRef](#)]
10. Wieland, M. Safety aspects of sustainable storage dams and earthquake safety of existing dams. *Engineering* **2016**, *2*, 325–331. [[CrossRef](#)]
11. Wang, G.; Wang, Y.; Lu, W.; Yu, M.; Wang, C. Deterministic 3D seismic damage analysis of Guandi concrete gravity dam: A case study. *Eng. Struct.* **2017**, *148*, 263–276. [[CrossRef](#)]
12. Song, L.; Wu, M.; Xu, Y.; Wang, J.-T. Seismic damage analysis of the outlet piers of arch dams using the finite element sub-model method. *Earthq. Eng. Eng. Vib.* **2016**, *15*, 617–626. [[CrossRef](#)]
13. Pani, P.; Bhattacharyya, S. Hydrodynamic pressure on a vertical gate considering fluid—Structure interaction. *Finite Elements Anal. Des.* **2008**, *44*, 759–766. [[CrossRef](#)]
14. Pani, P.; Bhattacharyya, S. Fluid—structure interaction effects on dynamic pressure of a rectangular lock-gate. *Finite Elements Anal. Des.* **2007**, *43*, 739–748. [[CrossRef](#)]
15. Løkke, A.; Chopra, A.K. Direct finite element method for nonlinear earthquake analysis of concrete dams: Simplification, modeling, and practical application. *Earthq. Eng. Struct. Dyn.* **2019**, *48*, 818–842. [[CrossRef](#)]
16. Fadaei Kermani, E.; Barani, G.; Ghaeini-Hessaroeeyeh, M. Prediction of cavitation damage on spillway using K-nearest neighbor modeling. *Water Sci. Technol.* **2014**, *71*, 347–352. [[CrossRef](#)] [[PubMed](#)]
17. Kumcu, S.Y. Investigation of flow over spillway modeling and comparison between experimental data and CFD analysis. *KSCE J. Civ. Eng.* **2017**, *21*, 994–1003. [[CrossRef](#)]
18. Pfister, M.; Duarte, R.; Müller, M.; De Cesare, G. Cavitation risk estimation at orifice spillway based on UVP and dynamic pressure measurements. In Proceedings of the 8th International Symposium on Ultrasonic Doppler Methods for Fluid Mechanics and Fluid Engineering, Dresden, Germany, 19–21 September 2012.

19. Luo, Y.Q.; Diao, M.J.; He, D.M.; Bai, S.X. Numerical simulation of aeration and cavitation in high dam spillway tunnels. *Adv. Water Sci.* **2012**, *23*, 110–116.
20. Frizell, K.W.; Renna, F.M.; Matos, J. Cavitation potential of flow on stepped spillways. *J. Hydraul. Eng.* **2012**, *139*, 630–636. [[CrossRef](#)]
21. Brusiewicz, K.; Sterpejkowicz-Wersocki, W.; Jankowski, R. Modal Analysis of a Steel Radial Gate Exposed to Different Water Levels. *Arch. Hydro-Eng. Environ. Mech.* **2017**, *64*, 37–47. [[CrossRef](#)]
22. ICOLD. *Neotectonics and Dams, Bulletin 112, Committee on Seismic Aspects of Dam Design*; ICOLD: Paris, France, 1998.
23. Peirovi, S.; Pourasghar, M.; Nejad, A.F.; Hassan, M.A. A study on the different finite element approaches for laser cutting of aluminum alloy sheet. *Int. J. Adv. Manuf. Technol.* **2017**, *93*, 1399–1413. [[CrossRef](#)]
24. Alipour, R.; Nejad, A.F.; Izman, S. The reliability of finite element analysis results of the low impact test in predicting the energy absorption performance of thin-walled structures. *J. Mech. Sci. Technol.* **2015**, *29*, 2035–2045. [[CrossRef](#)]
25. Nejad, A.F.; Chiandussi, G.; Moshrefzadeh, A.; Solimine, V.; Serra, A.; Rulfi, E. Modal Dynamic Analysis of a Synchronizer Mechanism: A Numerical Study. *Int. J. Mech. Eng. Robot. Res.* **2019**, *8*, 340–346. [[CrossRef](#)]
26. Perri, J.F.; Pestana, J.M. Ground motion analysis with the use of the short-time-response-spectrum. *J. Earthq. Eng.* **2017**, *21*, 384–410. [[CrossRef](#)]
27. Feng, J.J.H. Conversion between power spectrum and response spectrum and artificial earthquakes. *Earthq. Eng. Eng. Vib.* **1984**, *3*.
28. Falvey, H.T. *Cavitation in Chutes and Spillways*. 1990. Available online: https://www.researchgate.net/profile/Henry_Falvey/publication/236013942_Cavitation_in_Chutes_and_Spillways_Engineering_Monograph_No_42/links/59808b674585156238facfbd/Cavitation-in-Chutes-and-Spillways-Engineering-Monograph-No-42.pdf (accessed on 29 August 2020).
29. Xu, W.; Luo, S.; Zheng, Q.; Luo, J. Experimental study on pressure and aeration characteristics in stepped chute flows. *Sci. China Technol. Sci.* **2015**, *58*, 720–726. [[CrossRef](#)]
30. Song, D.; Wang, E.; Xu, J.; Liu, X.; Shen, R.; Xu, W. Numerical simulation of pressure relief in hard coal seam by water jet cutting. *Geomech. Eng.* **2015**, *8*, 495–510. [[CrossRef](#)]
31. Sreedhar, B.; Albert, S.; Pandit, A. Cavitation damage: Theory and measurements—A review. *Wear* **2017**, *372*, 177–196. [[CrossRef](#)]
32. Rutschmann, P.; Hager, W.H. Air entrainment by spillway aerators. *J. Hydraul. Eng.* **1990**, *116*, 765–782. [[CrossRef](#)]
33. De Michele, C.; Salvadori, G.; Canossi, M.; Petaccia, A.; Rosso, R. Bivariate Statistical Approach to Check Adequacy of Dam Spillway. *J. Hydrol. Eng.* **2005**, *10*, 50–57. [[CrossRef](#)]
34. Herrera-Granados, O.; Kosteki, S.W. Numerical and physical modeling of water flow over the ogee weir of the new Niedów barrage. *J. Hydrol. Hydromech.* **2016**, *64*, 67–74. [[CrossRef](#)]
35. Rice, C.E.; Kadavy, K.C. Model Study of a Roller Compacted Concrete Stepped Spillway. *J. Hydraul. Eng.* **1996**, *122*, 292–297. [[CrossRef](#)]
36. Santos, P.M.; Júlio, E.; Da Silva, V.D. Correlation between concrete-to-concrete bond strength and the roughness of the substrate surface. *Constr. Build. Mater.* **2007**, *21*, 1688–1695. [[CrossRef](#)]
37. Volkart, P.; Rutschmann, P. *Air Entrainment Devices (Air Slots)*; Eidgenössische Technische Hochschule: Zurich, Switzerland, 1984.
38. Kökpınar, M.A.; Göğüş, M. High-speed jet flows over spillway aerators. *Can. J. Civ. Eng.* **2002**, *29*, 885–898. [[CrossRef](#)]
39. Sattar, A.M.A.; Elhakeem, M.; Rezaie-Balf, M.; Gharabaghi, B.; Bonakdari, H. Artificial intelligence models for prediction of the aeration efficiency of the stepped weir. *Flow Meas. Instrum.* **2019**, *65*, 78–89. [[CrossRef](#)]
40. Ozkan, F.; Baylar, A.; Ozturk, M. *Discussion: Air Entrainment and Oxygen Transfer in High-Head Gated Conduits. Proceedings of the Institution of Civil Engineers-Water Management*; Thomas Telford Ltd.: London, UK, 2020.

